Organic Electronics 14 (2013) 723–729

Contents lists available at SciVerse ScienceDirect

Organic Electronics

journal homepage: www.elsevier.com/locate/orgel

Metal-anode-dependent spectra and efficiency in blue top-emitting organic light-emitting devices

Jing Wang [a,b], Wenyu Ji [a,*], Hongbo Zhu [a], Dandan Zhang [c,*]

[a] State Key Laboratory of Luminescence and Applications, Changchun Institute of Optics, Fine Mechanics and Physics, Chinese Academy of Sciences, Changchun 130033, People's Republic of China
[b] School of Physics and Technology, University of Jinan, Jinan 250022, People's Republic of China
[c] Jiangsu Key Laboratory for Carbon-Based Functional Materials and Devices, Institute of Functional Nano and Soft Materials (FUNSOM), Soochow University, Suzhou 215123, China

ARTICLE INFO

Article history:
Received 28 September 2012
Received in revised form 19 December 2012
Accepted 22 December 2012
Available online 5 January 2013

Keywords:
TEOLED
Electroluminescence
Microcavity
Angle-independent
Phase shift on reflectance

ABSTRACT

In this study, the blue top-emitting organic light-emitting devices (TEOLEDs) with different metal anodes are fabricated. The effect of different anode materials on the spectra and efficiency of blue TEOLEDs is studied. We demonstrate that Al is a more suitable anode material for blue TEOLEDs due to its larger phase shift on reflectance (PSR) than the other common metal materials, such as Ag and Au. The influence of light outcoupling layer (LOL) on the transmittance and PSR of cathode is also investigated to obtain the optimum condition for devices. Angle-independent electroluminescence (EL) spectra are obtained in blue TEOLEDs for each metal anode but the device with Al anode possesses higher efficiency and much thicker organic layers, which is beneficial to the lifetime of the device. These results offer a practicable platform for the realization of TEOLEDs based full-color displays and lightings.

1. Introduction

Top-emitting organic light-emitting devices (TEOLEDs) are of interest recently due to the light coupling out from top side allowing TEOLEDs onto arbitrary substrates, such as silicon and foil substrates. TEOLEDs possess higher aperture ratio (AR) than the usual bottom-emitting devices [1–3], which results in TEOLEDs more suitable for active matrix (AM) display. AM OLED display has many advantages, such as high resolution, fast response, low power consumption, and large display area. To obtain a constant and uniform drive current in AM OLEDs, pixel driving circuits commonly include four or more backplane thin film transistors (TFTs) in combination with one capacitor [4,5]. However, a large number of TFTs fabricated on the substrate will invariably reduce the AR of each pixel in a bottom-emitting OLED (BEOLED). Furthermore, the light is emitted through a transparent indium tin oxide (ITO) coated glass substrate in BEOLEDs, which leads to significant waveguiding losses. Fortunately, TEOLEDs are structurally unaffected by the number of TFTs integrated on the substrate because the light emits from the top side and are particularly suitable for high-resolution AM displays.

To date, among the three primary colors, both top-emitting and bottom-emitting blue OLEDs are currently lagging behind green and red OLEDs in terms of device performances. The ability to produce high efficient blue TEOLEDs is very crucial to achieving the TEOLEDs based full color displays and lighting sources. The phosphorescent emitters can harvest both the singlet and triplet excitons, leading to the potential for achieving 100% internal quantum efficiency [6]. This important breakthrough has opened up opportunity to fabricate high efficient blue phosphorescent TEOLEDs. However, realization of a high-performance and angle-independent blue TEOLEDs is still a major obstacle

* Corresponding authors.
E-mail addresses: jlu_jwy@163.com (W. Ji), zhangdandan163@126.com (D. Zhang).

1566-1199/$ - see front matter © 2012 Elsevier B.V. All rights reserved.
http://dx.doi.org/10.1016/j.orgel.2012.12.021

to overcome. Currently, the development of phosphorescent iridium complex based emission layers, such as iridium(III) bis[(4,6-difluorophenyl) pyridinato-N,C20]picolinate (FIrpic) with the emission from 425 nm to 600 nm has received much attention [7–9]. Here, we also fabricated the blue TEOLEDs based on FIrpic emitter and investigated the effect of materials and structure of electrodes on the device performances.

Blue TEOLEDs have been widely investigated, but the angle-dependent emission is inevitable due to microcavity effect in the devices consisted of organic layers sandwiched between high reflective anode and semitransparent cathode. It can be overcome by applying a light outcoupling layer (LOL) on the top cathode to increase the transmission of the top electrode and reduce the microcavity effects [10–12]. The resonant wavelengths (RWs) of the microcavity for normal incidence are determined by the Fabry–Perot peak condition [13]:

$$\varphi_{anode}(0,\lambda)+\varphi_{cathode}(0,\lambda)+2m\pi=\sum_i\frac{4\pi d_i n_i(\lambda)}{\lambda} \quad (1)$$

where λ is the emission wavelength, $\varphi_{\mathrm{cathode}}(0,\ \lambda)$ and $\varphi_{\mathrm{anode}}(0,\ \lambda)$ are the wavelength-dependent phase shift on reflection (PSR) for top cathode and bottom anode, respectively, m is an integer that defines the mode number of the cavity, $n_i(\lambda)$ and d_i are the refractive index and thickness of ith organic layer, respectively. Considering the operating voltage, the thickness of the device is often less than 130 nm. Consequently, the value of m must be 0 to meet the peak condition. In terms of Eq. (1), a shorter RW needs a thinner device. Generally, the thickness of the blue TEOLED is about 80 nm, which is smaller than the red and green TEOLEDs, more than 100 nm. As we know, it is disadvantageous to the device lifetime when the device thickness is too thin. At present, the lifetime of blue TEOLED is shorter than that of red or green ones and the device thickness should play a crucial role. How to fabricate a blue TEOLED having similar thickness to the red or green TEOLEDs is still an open problem. Utilizing an electrode with high enough PSR is a route to achieve this goal according to Eq. (1) and can be easily achieved because the PSR is obviously different for various metal films [14]. In addition, the reflectance and transmittance of the electrodes also play an important role in cavity devices since it affects the cavity strength as well as the outcoupled spectra. Here, we will consider all of these parameters and investigate their effect on the device performances.

For a certain RW, in terms of Eq. (1), the total thickness of the device is determined by the PSR of two electrodes. To evaluate the effect of electrode on device thickness, different metal anodes have been used in our blue TEOLEDs. Considering the devices with two different anodes but the same cathode, the difference of the device thickness for the same RW λ_0 is obtained from Eq. (1):

$$\varphi_{m1}(0,\lambda_0)-\varphi_{m2}(0,\lambda_0)=\frac{4\pi d_{m1}n_{\lambda_0}}{\lambda_0}-\frac{4\pi d_{m2}n_{\lambda_0}}{\lambda_0} \quad (2)$$

$$(d_{m1}-d_{m2})=\frac{\lambda_0}{4\pi n_{\lambda_0}}\cdot[\varphi_{m1}(0,\lambda_0)-\varphi_{m2}(0,\lambda_0)] \quad (3)$$

where d is the total thickness of the active layers between anode and cathode, φ is the PSR, the subscripts $m1$ and $m2$ represent different metal anodes. Fig. 1a shows the PSR for different metal films, Ag, Al, and Au, with a thickness of 120 nm. The calculation for PSR is based on the transfer matrix theory [15], the incidence medium is 4, 4-N, N-dicarbazole-biphenyl (CBP). As can be seen, the PSR is very different for various metal films and the Al film has the largest PSR in the visible range from 380 nm to 780 nm, which indicates that the device thickness with Al anode will be larger than that based on Au or Ag anode at the same resonant peak in terms of Eq. (3). For example, considering the device with resonant peak of 450 nm, where the PSR is 2.5 and 1.9 for Al and Ag (Au), respectively. The refractive index of 1.7 is used for organic materials and the difference of the device thickness is calculated from Eq. (3):

$$(d_{m1}-d_{m2})=\frac{450}{4\times3.14\times1.7}\cdot[2.5-1.9]=12.6\ \mathrm{nm}$$

This result indicates that the device thickness with Al anode is 12.6 nm thicker than that of Ag (Au) based device. Fig. 1b shows the reflectance and absorption spectra for the 120 nm Al, Ag and Au films. We can see that high reflectance and low absorptance are obtained for the Al and Ag films, which is of benefit to the efficiency of the

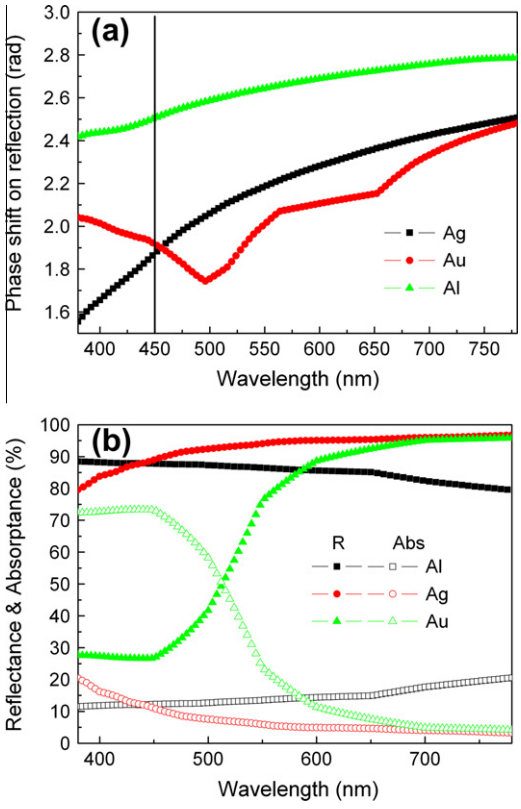

Fig. 1. (a) The phase shift on reflection for Ag, Au and Al. (b) The reflection and absorption spectra for Ag, Au and Al.

TEOLEDs. In contrary, Au film possesses the lowest reflectance and highest absorptance in the blue region, which will decrease the efficiency of blue device.

In terms of Eq. (1), the PSR of cathode also plays an important role in determining the device thickness. Fig. 2a shows the calculated PSR of 17 nm Ag cathode and composite cathodes consisted of 17 nm Ag combining with different LOLs, tris (8-hydroxyquinoline) aluminum (Alq_3, 40 nm), MoO_3 (35 nm) and TiO_2 (28 nm) and the refractive indices of Alq_3, MoO_3 and TiO_2 are shown in Fig. 2b. As can be seen, the Ag cathode has smaller PSR in blue region and the PSR of the composite cathode increases with a higher refractive index LOL introduced. As discussed above, higher PSR of electrode is of benefit to fabricate a thicker device and here we will select the material with higher refractive index as the LOL. The optimum thickness of each LOL is obtained through calculating the transmittance of the cathodes as shown in Fig. 2c. The single layer Ag cathode has the lowest transmittance. However, this drawback has been overcome by applying a LOL as reported [10–12,16]. Generally, the optical properties of ITO are directly measured, which are very different to the actual case that the light is emitted from organic layers in TEOLEDs. Here, we also calculated the optical properties of ITO for the comparison with that of cathodes discussed above. The transmittance of cathodes with MoO_3 and TiO_2 as the LOL is similar, more than 80% in visible region, lower than that of ITO but higher than that of Alq_3 as the LOL in the range of 425–780 nm. The increase of transmittance through the top electrode will reduce microcavity effect and alleviate the viewing angle dependence of the emission spectra. Consequently, MoO_3 and TiO_2 should be the suitable LOL materials. Fig. 2d shows the calculated reflectance of all the cathodes and ITO. It is valuable to note that the electrode with a higher transmittance usually possesses a lower reflectance. High transmittance and low reflectance are beneficial to alleviate the undesired microcavity effect, which is considered problematic, particularly for angular color non-uniformity (angle-dependence of spectra). Here, considering the properties of the cathode and the compatibility to the processes of fabricating TEOLEDs, we select MoO_3 film as the LOL due to the ease of processing (low evaporation temperature, melting point ≈795 °C) relative to that of TiO_2 film which maybe needs a radio-frequency sputtering processing. The incidence medium is 1, 3, 5-Tri(1-phenyl-1H-benzo[d]imidazol-2-yl)phenyl (TPBi) for the calculation in Fig. 2. The optical constants of the organic materials, LOL materials and ITO were measured using a variable angle spectroscopic ellipsometer.

With these data in hand, we tried to fabricate blue TEOLEDs consisted of glass/anode (120 nm)/MoO_3 (2 nm)/4, 4-N, N- dicarbazole-biphenyl (CBP, *x* nm)/mCP:FIrpic (12 wt.%, 30 nm)/1, 3, 5-Tri(1-phenyl-1H-benzo[d]imidazol-2-yl)phenyl (TPBi, *y* nm)/LiF (1 nm)/Al (1 nm)/Ag(17 nm)/MoO_3 (35 nm). Here, *x* is 28 and *y* is

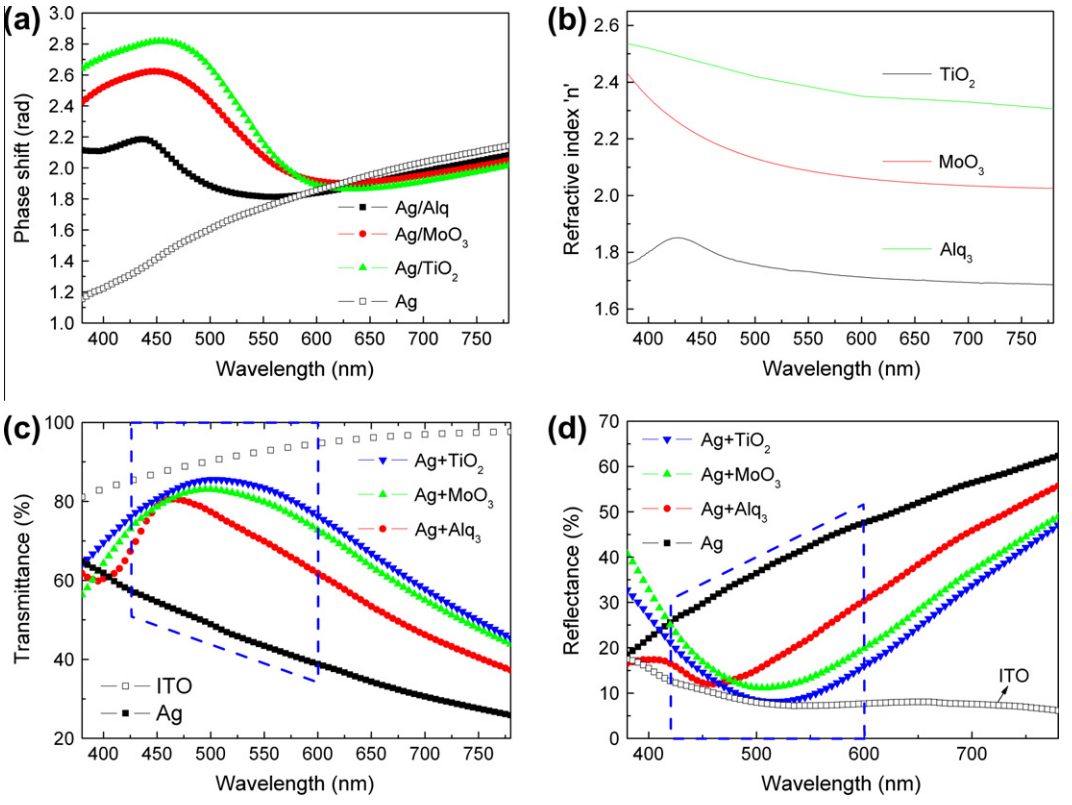

Fig. 2. (a) The phase shift on reflection for different cathodes, (b) the refractive indices of Alq_3, MoO_3, and TiO_2, (c) the transmittance and (d) reflectance of cathodes and ITO.

40 for Al anode based device and x is 23 and y is 30 for Ag and Au anodes based devices. For comparison, the BEOLED was also fabricated with the same structure of glass/ITO (180 nm)/MoO_3 (2 nm)/ CBP (30 nm)/mCP:FIrpic (30 nm)/TPBi (40 nm)/LiF (1 nm)/Al (120 nm). The mCP is N,N′-dicarbazolyl-3,5-benzene. FIrpic and mCP were purchased from Luminescence Technology Corporation and all other materials were purchased from Sigma–Aldrich. The materials were used as received without any processing. All films were deposited at pressure below 4×10^{-6} Torr. Detailed processes of fabrication and measurement for OLEDs have been described in our previous paper [17].

Fig. 3a shows the calculated round-trip phase changes for 85 and 100 nm organic layers sandwiched between cathode and anode $\left(\text{i.e., } \varphi_1(0,\lambda) = \sum_i \frac{4\pi d_i n_i(\lambda)}{\lambda}\right)$, and the phase changes at two reflective electrodes (i.e., $\varphi_2(0,\lambda) = \varphi_{cathode}(0,\lambda) + \varphi_{anode}(0,\lambda)$, φ_{anode} $(0,\lambda)$ and φ_{anode} $(0,\lambda)$ are the wavelength-dependent phase changes on reflection from top cathode and bottom anode, respectively) Here, three anode materials, Ag, Au, and Al, are chosen and incidence mediums are TPBi and CBP in the calculations for cathode and anode, respectively. The intersections of $\varphi_{anode}(0,\lambda)$ and $\varphi_{anode}(0,\lambda)$ are the RWs of the devices. As can be seen, when the thickness of organic layers is 85 nm, Al based device exhibits a shorter RW,

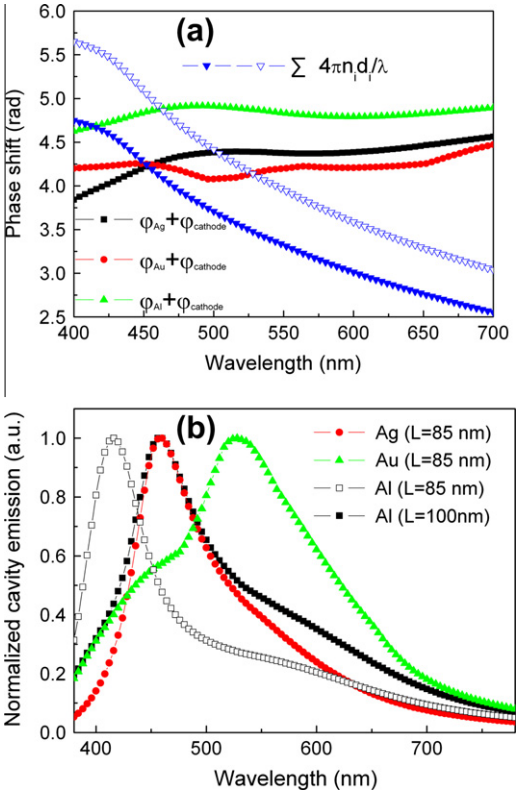

Fig. 3. (a) The calculated round-trip phase changes for 80 and 100 nm organic layers between two electrodes and the phase changes on two electrodes. (b) The calculated forward directed cavity emission for different anodes.

∼414 nm, than that of Ag or Au based devices, ∼452 nm. the With the thickness of organic layers increasing to 100 nm, the RW of Al based device reaches about 460 nm. These results are in agreement well with that discussed above. In order to clarify the microcavity effect in the devices, we calculated the cavity emission by considering wavelength-independment instrsinc luminescence spectra of the emitter [18], as shown in Fig. 3b. The RWs of cavity emission are in agreement with the results depicted in Fig. 3a except for Au anode based device. The large discrepancy for Au based device is due to the low reflectance and high absorptance of Au anode in the range of 400–520 nm. The high absorptance of Au anode has the similar effect as the filter that the emission in the range of 400–520 nm is absorbed, consequently resulting in a cavity emission with a peak at about 527 nm and a shoulder peak of about 454 nm. These results also indicates that not only the PSR but also the reflectance/absorptance of the anodes influence the spectra of TEOLEDs greatly. Consequently, it is very essential to consider all the parameters for the optical design on TEOLEDs.

Fig. 4a–c shows the normalized EL spectra of devices with Ag, Au, and Al anodes, respectively, and all of the emission spectra are almost angle-independent. The normalized EL spectrum of BEOLED is also plotted to clarify the effect of microcavity on the spectra of TEOLEDs. As can be seen, the microcavity narrows the half width at half maximum (FWHM) of emission spectra in Ag and Al anodes based devices. The FWHM of emission spectra in Au anode based device is increased a little relative to that of BEOLED, which is attributed to the enhanced emission near 527 nm as depicted in Fig. 3b. The FWHM is 61 nm for the spectrum of BEOLED, and it is ∼40 nm for Ag and Al based devices and 74 nm for Au based device. We also explained the FWHM of emission spectrum by the following equation [19,20]:

$$FWHM = \frac{\lambda^2}{2L} \times \frac{1 - \sqrt{R_1 R_2}}{\pi (R_1 R_2)^{1/4}} \tag{4}$$

where R_1 and R_2 are the reflectance of the two electrodes and L is the optical length between the two electrodes. As implied from Eq. (4), a smaller R_1 and R_2 are preferred to obtain larger FWHM in TEOLEDs. In our devices, the cathode reflectance R_1 is uniform in all the TEOLEDs due to the same cathode structure, but the reflectance of Au anode is very low, resulting in a larger FWHM for Au based TEOLED.

As we know, TEOLEDs combined with driving circuit) such as organic thin film transistor (OTFT) or complementary metal oxide semiconductor (CMOS)) is the most effective method to obtain high-resolution displays. Thus, TEOLEDs with appropriate electrode will simplify the fabrication process of the integrated device and be compatible with the fabrication of driving circuit. Although Au or Al is usually used as electrode in OTFT [21–23] or CMOS [24–26], the Al is the optimum choice as the anode material in blue TEOLED considering the Al based device has higher efficiency than that of Au based device as shown in Fig. 5b. In Fig. 4d, we calculated the emisson of Al based device at different viewing angle of 0°, 15°, 30°, 45°, 60° following

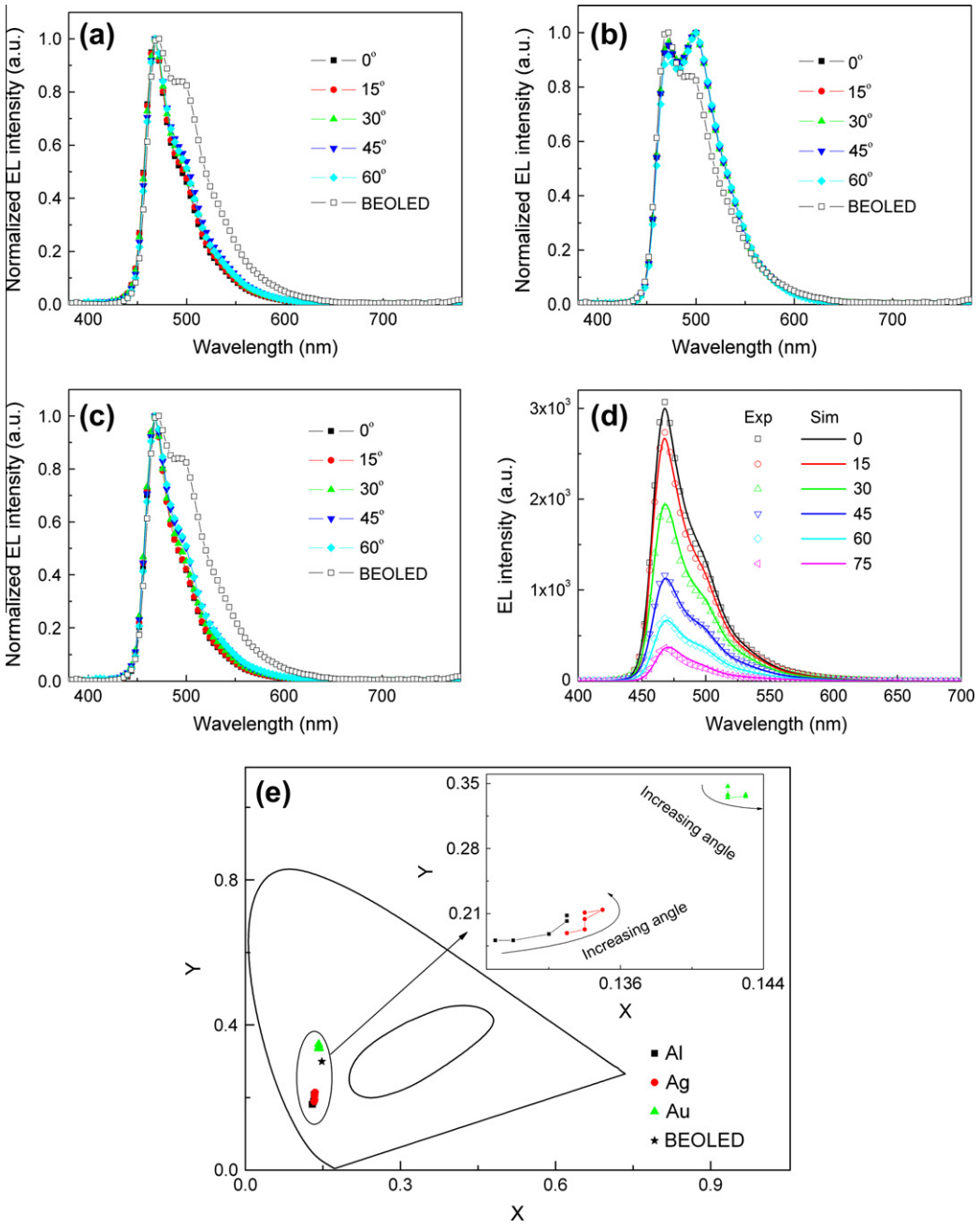

Fig. 4. The EL spectra at different viewing angle for (a) Ag, (b) Au and (c) Al anode. (d) The normalized EL spectra by calculating and measuring of the device with Al anode. (e) The CIE coordinates of all the TEOLEDs, an enlarged image in the upper right corner is shown in the inset.

the approach reported by Deppe et al. [27], which was excellent agreement with the experiment results.

The Commission Internationale de l'Eclairage (CIE) coordinates of TEOLEDs at different viewing angles are shown in Fig. 4e. We can see that the CIE coordinates are almost constant. An enlarged view of the CIE coordinates for different viewing angle is shown in the inset. The maximum differences for CIE coordinates in the range of 0–60° are (0.002, 0.025), (0.001, 0.012), and (0.004, 0.027) for Ag, Au, and Al anodes based blue devices, respectively. The change is less than 0.4% for coordinate *x* and 3% for coordinate *y*. To our knowledge, these are the stablest blue TEOLEDs reported to date. The CIE coordinates for forward direction are (0.133, 0.189), (0.143, 0.338), and (0.129, 0.181) for Ag, Au, and Al anodes based blue devices, respectively, and the CIE coordinates of BEOLED is (0.148, 0.299), as shown in Fig. 4e. As can be seen, the color saturation of Al and Ag based devices is improved relative to the BEOLED, which indicates higher color purity can be achieved in Ag and Al based TEOLEDs. The color purity is

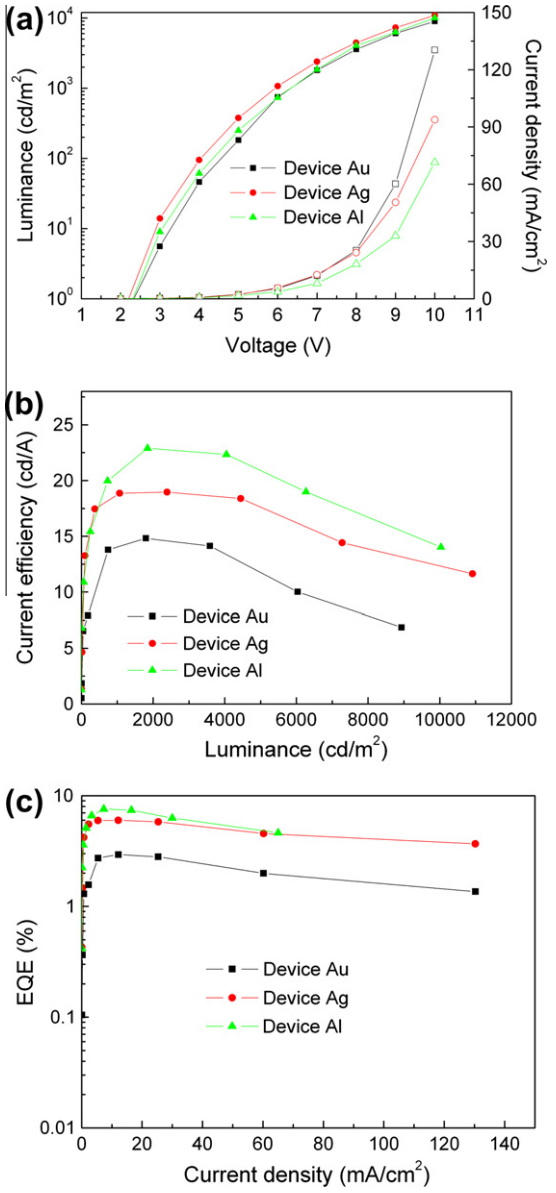

Fig. 5. (a) The luminance–voltage–current density, (b) luminance-efficiency and (c) EQE characteristics of TEOLEDs.

a very important parameter in display and lighting applications. However, the color saturation of Au based devices becomes poorer than that of the BEOLED due to the broadened EL spectra in Au based TEOLED.

Fig. 5a shows the luminance–voltage–current density characteristics of all the TEOLEDs. At the same voltage, the current density increases according to Al, Ag, and Au sequence, which is due to the increase of work function, ~4.10, ~4.73, and ~5.20 V for Al, Ag, and Au, respectively [28]. In addition, the thicker Al based TEOLED also leads to the lower current density. The device with Ag anode possesses the highest luminance in three devices at the same voltage, which is attributed to the efficient hole-injection and high reflectance of Ag anode. Fig. 5b shows

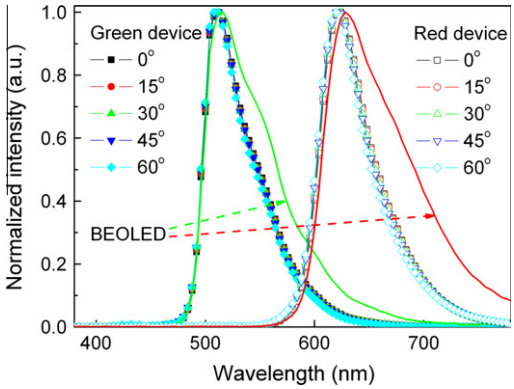

Fig. 6. The simulated spectra for green and red devices at viewing angles from 0° to 60°.

the efficiency–luminance characteristics of three blue devices. The maximum efficiencies are 19.0, 14.8, and 22.9 cd/A for Ag, Au, and Al anodes based blue devices, respectively, with the corresponding roll-off of 7.4%, 20.9%, and 8.7% up to a luminance of 5000 cd/m^2. We can find that the Al based device shows the highest efficiency in all the devices, which may be due to the better charge balance in Al based device because of the reduced hole-injection from the anode. In addition, the high absorption of Au anode results in the loss of the light inside the device and reduces the device efficiency. The external quantum efficiencies (EQEs) are calculated by measuring the emission spectra and the intensities at different emission angles. As shown in Fig. 5c, the peak EQE for Au, Ag, and Al based TEOLEDs is 6.0%, 7.6%, and 2.9%, respectively.

For full-color display applications, the technique of patterning using a shadow mask and a three-step red–green–blue (RGB) subpixel deposition technique is yet proven as a viable high-volume manufacturing technique. Thus, it is more valuable to fabricate green and red TEOLEDs with the similar structure to achieve full color flat panel displays. We have stimulated the emission spectra of the green and red TEOLEDs with the same cathode structure to that of present blue TEOLED, which ensures the compatibility and simplicity in the fabrication of future TEOLED based full color flat panel displays. Fortunately, we also obtained angle-independent emission spectra as shown in Fig. 6. Details of the device structure and the fabrication of the corresponding devices will be the topic of future research. In addition, the power efficacy of a microcavity TEOLED is measured by using an integrating sphere to capture all of the emitted light, which will also be investigated in future.

In conclusion, we have investigated the influence of anode materials (Ag, Au, and Al) on the performances of blue TEOLEDs with Firpic as the emitter through theory and experiment. A much thicker (100 nm) blue TEOLED is obtained by utilizing Al anode due to its larger PSR than that of Ag and Au anodes. In addition, the optical properties of the Ag cathodes with and without LOL are also simulated. High transmittance and PSR are obtained by introducing the LOL, especially, the transmittance and PSR increase with a higher refractive index LOL material introduced.

These results provide new guides for device design that can be used to improve the performance of TEOLEDs and accelerate the realization of TEOLED-based lighting sources and full-color panel displays.

Acknowledgement

This research was supported by the National Natural Science Foundation of China (Nos. 61205025 and 61205033).

References

[1] L.S. Hung, C.W. Tang, M.G. Mason, P. Raychaudhuri, J. Madathil, Application of an ultrathin LiF/Al bilayer in organic surface-emitting diodes, Appl. Phys. Lett. 78 (2001) 544.
[2] Z.Y. Xie, L.S. Hung, F.R. Zhu, A flexible top-emitting organic light-emitting diode on steel foil, Chem. Phys. Lett. 381 (2003) 691.
[3] C.C. Wu, C.W. Chen, C.L. Lin, C.J. Yang, Advanced organic light-emitting devices for enhancing display performances, J. Display Technol. 1 (2005) 248.
[4] J.H. Lee, W.J. Nam, S.M. Han, M.K. Han, OLED pixel design employing a novel current scaling scheme, Dig. Tech. Pap. – Soc. Inf. Disp. Int. Symp. 3 (4) (2003) 490.
[5] J.C. Goh, C.K. Kim, J. Jang, A novel pixel circuit for active-matrix organic light-emitting diodes, Dig. Tech. Pap. – Soc. Inf. Dsisp. Int. Symp. 3 (4) (2003) 494.
[6] C. Adachi, M.A. Baldo, M.E. Thompson, S.R. Forrest, Nearly 100% internal phosphorescence efficiency in an organic light-emitting device, J. Appl. Phys. 90 (2001) 5048.
[7] H. Liu, G. Cheng, D.H. Hu, F.Z. Shen, Y. Lv, G.N. Sun, B. Yang, P. Lu, Y.G. Ma, A highly efficient, blue-phosphorescent device based on a wide-bandgap host/flrpic: rational design of the carbazole and phosphine oxide moieties on tetraphenylsilane, Adv. Funct. Mater. 22 (2012) 2830.
[8] S.L. Gong, X. He, Y.H. Chen, Z.Q. Jiang, C. Zhong, D.G. Ma, J.G. Qin, C.L. Yang, Simple CBP isomers with high triplet energies for highly efficient blue electrophosphorescence, J. Mater. Chem. 22 (2012) 2894.
[9] J. Xie, C. Chen, S.F. Chen, Y. Yang, M. Shao, X. Guo, Q.L. Fan, W. Huang, Blue top-emitting organic light-emitting devices based on wide-angle interference enhancement and suppression of multiple-beam interference, Org. Electron. 12 (2011) 322.
[10] X.L. Zhu, J.X. Sun, X.M. Yu, M. Wong, H.S. Kwok, High-performance top-emitting white organic light-emitting devices, Jpn. J. Appl. Phys. 46 (2007) 4054.
[11] M. Thomschke, R. Nitsche, M. Furno, K. Leo, Optimized efficiency and angular emission characteristics of white top-emitting organic electroluminescent diodes, Appl. Phys. Lett. 94 (2009) 083303.
[12] S.F. Hsu, C.C. Lee, S.W. Hwang, C.H. Chen, Highly efficient top-emitting white organic electroluminescent devices, Appl. Phys. Lett. 86 (2005) 253508.
[13] A.B. Djurišić, A.D. Rakić, Organic microcavity light-emitting diodes with metal mirrors: dependence of the emission wavelength on the viewing angle, Appl. Opt. 41 (2002) 7650.
[14] W.Y. Ji, L.T. Zhang, T.Y. Zhang, W.F. Xie, H.Z. Zhang, High-contrast and high-efficiency microcavity top-emitting white organic light-emitting devices, Org. Electron. 11 (2010) 202.
[15] C.L. Mitsas, D.I. Siapkas, Generalized matrix-method for analysis of coherent and incoherent reflectance and transmittance of multilayer structures with rough surfaces, interfaces, and finite substrates, Appl. Opt. 34 (1995) 1678.
[16] M.T. Lee, M.R. Tseng, Efficient, long-life and Lambertian source of top-emitting white OLEDs using low-reflectivity molybdenum anode and co-doping technology, Curr. Appl. Phys. 8 (2008) 616.
[17] W.Y. Ji, L.T. Zhang, W.F. Xie, Improving efficiency roll-off in phosphorescent OLEDs by modifying the exciton lifetime, Opt. Lett. 37 (2012) 2019.
[18] P. Freitag, S. Reineke, S. Olthof, M. Furno, B. Lüssem, K. Leo, White top-emitting organic light-emitting diodes with forward directed emission and high color quality, Org. Electron. 11 (2010) 1676.
[19] E.F. Schubert, N.E.J. Hunt, M. Micovic, R.J. Malik, D.L. Sivco, A.Y. Cho, G.J. Zydzik, Highly efficient light-emitting-diodes with microcavities, Science 265 (1994) 943.
[20] A. Dodabalapur, L.J. Rothberg, T.M. Miller, E.W. Kwock, Microcavity effects in organic semiconductors, Appl. Phys. Lett. 64 (1994) 2486.
[21] N.T. Salim, K.C. Aw, W. Gao, Z.W. Li, B. Wright, ZnO as a dielectric for organic thin film transistor-based non-volatile memory, Microelectron. Eng. 86 (2009) 2127.
[22] C.H. Li, F. Pan, F. Zhu, D. Song, H. Wang, D.H. Yan, Very low hysteresis organic thin-film transistors, Semicond. Sci. Technol. 24 (2009) 085009.
[23] D.J. Yun, S.H. Lim, T.W. Lee, S.W. Rhee, Fabrication of the flexible pentacene thin-film transistors on 304 and 430 stainless steel (SS) substrate, Org. Electron. 10 (2009) 970.
[24] M. Fischer, M. Nägele, D. Eichner, C. Schö11horn, R. Strobel, Integration of surface-micromachined polysilicon mirrors and a standard CMOS process, Sensor Actuat. A: Phys. 52 (1996) 140.
[25] K.A. Honer, G.T.A. Kovacs, Integration of sputtered silicon microstructures with pre-fabricated CMOS circuitry, Sensor Actuat. A: Phys. 91 (2001) 386.
[26] L.S. Pakula, H. Yang, H.T.M. Pham, P.J. French, P.M. Sarro, Fabrication of a CMOS compatible pressure sensor for harsh environments, J. Micromech. Microeng. 14 (2004) 1478.
[27] D.G. Deppe, C. Lei, C.C. Lin, D.L. Huffaker, Spontaneous emission from planar microstructures, J. Mod. Opt. 41 (1994) 325.
[28] S. Toyoshima, K. Kuwabara, T. Sakurai, T. Taima, K. Saito, H. Kato, K. Akimoto, Electronic structure of bathocuproine on metal studied by ultraviolet photoemission spectroscopy, Jpn. J. Appl. Phys. 46 (2007) 2692.